Available online at www.sciencedirect.com
ScienceDirect
International Journal of Heat and Mass Transfer 50 (2007) 2451–2462
International Journal of HEAT and MASS TRANSFER
www.elsevier.com/locate/ijhmt

Natural convection in triangular enclosures with protruding isothermal heater

Yasin Varol [a,*], Hakan F. Oztop [b], Tuncay Yilmaz [c]

[a] Department of Mechanical Engineering, Vanderbilt University, Nashville, TN 37235, USA
[b] Department of Mechanical Engineering, Firat University, 23119 Elazig, Turkey
[c] Department of Mechanical Engineering, Cukurova University, 01330 Adana, Turkey

Received 8 September 2006; received in revised form 4 December 2006
Available online 13 March 2007

Abstract

Natural convection heat transfer from a protruding heater located in a triangular enclosure has been analyzed numerically. Temperature of inclined boundary of the triangle is lower than the temperature of the heater, which has constant temperature boundary condition. The remaining walls are insulated. The study is formulated in terms of the vorticity-stream function procedure and numerical solution was performed using the finite difference method. Air was chosen as working fluid with $Pr = 0.71$. Governing parameters, which are effective on flow field and temperature distribution, are; Rayleigh number, aspect ratio of triangle enclosure, dimensionless height of heater, dimensionless location of heater and dimensionless width of heater. Streamlines, isotherms, velocity profiles, local and mean Nusselt numbers are presented. It is found that all parameters related with geometrical dimensions of the heater are effective on temperature distribution, flow field and heat transfer.

Keywords: Protruding heater; Natural convection; Triangle enclosure; Heat transfer

1. Introduction

Natural convection flow and heat transfer in different geometrical enclosures have been the topic of many research engineering studies. These studies consist of various technological applications such as solar collectors, building heating and ventilation, cooling electronical devices [1–3].

Protruding electronical heaters in non-rectangular enclosures can be used in PCs, monitors or TVs. Due to inclination surface of these devices, a protruding heater located triangular can be seen for circuit elements. Solution of natural convection in different shaped enclosures without partition or fin was studied by Tzeng et al. [4] and Asan and Namli [5,6], Akinsete and Coleman [7], Ridouane et al. [8] and Varol et al. [9,10].

Application and solution of flush mounted heater on the wall of enclosure is easier than protruding heater from the numerical analysis point of view as given in the most of the studies [11–13], partition was used as control element or heater for heat transfer and fluid flow. Dagtekin and Oztop [14] studied the natural convection by heated partitions with different heights within an enclosure. They used finite volume method using non-staggered grid to solve governing equations. They observed that as the partition's height increases, the mean Nusselt number increases. Also they found that the position of partitions has more effects on fluid flow than heat transfer. Similar applications were performed by Chuang et al. and Bhoite et al. [15,16]. Ben-Nakhi and Chamkha [17] solved the natural convection in inclined and insulated partitioned enclosures formulating vorticity-stream function procedure. They showed that as the dimensionless partition height increases, the flow velocity within the partitioned enclosure decreases resulting in less wall heat transfer. Yucel and Ozdem [18]

* Corresponding author. Tel.: +1 615 419 2734; fax: +1 615 343 6687.
E-mail address: ysnvarol@gmail.com (Y. Varol).

0017-9310/$ - see front matter © 2007 Elsevier Ltd. All rights reserved.
doi:10.1016/j.ijheatmasstransfer.2006.12.027

Nomenclature

AR	cavity aspect ratio, $=H/L$
c	dimensionless heater position
g	gravitational acceleration, m/s^2
Gr	Grashof number
h	dimensionless heater height
H	height of triangle, m
L	length of bottom wall of triangle, m
n	normal direction on a cavity wall
Nu	mean Nusselt number
Pr	Prandtl number
Ra	Rayleigh number
T	temperature, K
u, v	axial and radial velocities, m/s
U, V	non-dimensional axial and radial velocities
w	dimensionless heater width
X, Y	non-dimensional coordinates

Greek symbols

υ	kinematic viscosity, m^2/s
θ	non-dimensional temperature
Ω	non-dimensional vorticity
β	thermal expansion coefficient, 1/K
α	thermal diffusivity, m^2/s
Ψ	non-dimensional stream function

Subscripts

c	cold
h	hot

studied the natural convection in partially divided enclosures and they indicated that the mean Nusselt number decreases with the increasing of the height of partitions. Shi and Khodadadi [19] and Tasnim and Collins [20] studied the laminar natural convection in a square cavity due to a thin fin on the hot wall using different numerical techniques. They observed that placing an isothermal horizontal fin on the left hot wall of a differentially heated cavity generally modifies the clockwise rotating primary vortex that is established due to natural convection. Depending on the Rayleigh number, length of the fin and its position, a number of recirculation regions can be formed above and under the fin. Also, they obtained Nusselt number correlation. Bilgen [21] investigated the turbulent natural convection in an enclosure with divided a partition. Recently, Bilgen [22] conducted a study for conjugate heat transfer in a thin fin mounted enclosure at different conductivity ratio, Rayleigh number and geometrical parameter of the fin. He found that Nusselt number is an increasing function of Rayleigh number and a decreasing function of fin length and relative conductivity ratio. He proposed the fin as a control parameter and indicated that the heat transfer may be suppressed up to 38% by choosing appropriate thermal and geometrical fin parameter. Moukalled and Acharya [23] made a numerical investigation of natural convection in a trapezoidal enclosure (representing attic spaces) with offset baffles with two thermal boundary conditions representing summer-like and winterlike conditions. They obtained the maximum reduction in heat transfer for the position of one at the right of top wall and the other at the left side of the bottom wall. Similar study was performed by the same authors for single baffle inserted trapezoidal enclosure [24]. Also, other studies in the literature focused on protruding heaters [25–28] or coolers [29] for square or rectangular enclosures.

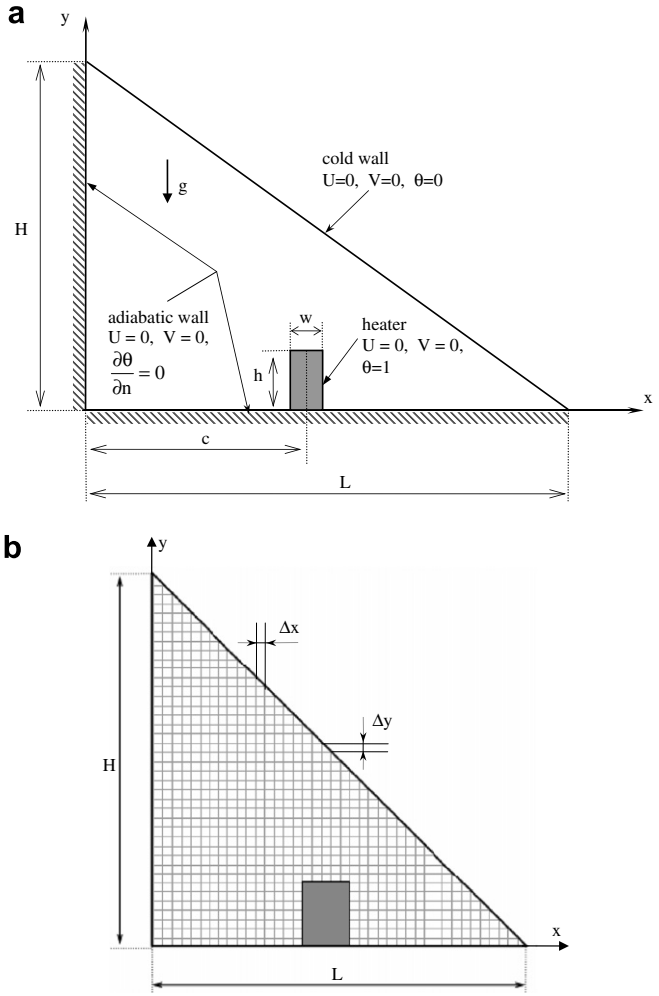

Fig. 1. (a) A schematic of the system, (b) grid distribution.

The main purpose of this study is to investigate the laminar natural convection heat transfer and fluid flow due to

insertion of heated protruding element which represents electronic element in triangular enclosure for laminar, two-dimensional flow. The review given above shows that, natural convection in heater located inside a triangular enclosure has not been investigated yet. Various Rayleigh number, height of the heater, heater width, heater location, aspect ratio of the triangular enclosure will be considered in this work.

2. Enclosure geometry with heater

The schematic configuration of a two-dimensional triangular enclosure with a rectangular heater on the bottom wall is shown in Fig. 1a. In this configuration, triangular enclosure with bottom wall of length, L and vertical wall is considered of height, H. Thus, an aspect ratio can be defined as the ratio of the height of vertical wall to length of bottom wall ($AR = H/L$). The rectangular heater kept at a constant temperature of T_h, width w and height h. The inclined wall is fixed at low isothermal of T_c. The vertical wall and remaining parts of the bottom walls are insulated.

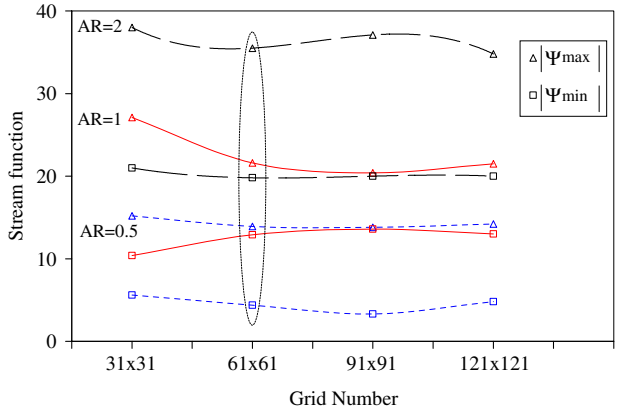

Fig. 2. Variation of stream function with different grid distribution for different aspect ratios.

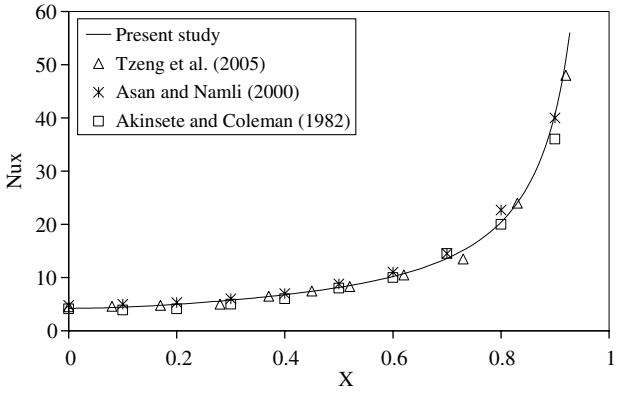

Fig. 3. Comparison of local Nusselt numbers with previous studies.

3. Equations

The system was considered to be two-dimensional, incompressible, steady-state, Newtonian and the Boussinesq approximation was applied for fluid with constant physical properties. It is assumed that the radiation effect can be taken to be negligible. The gravitational acceleration acts in the negative y-direction. Dimensionless

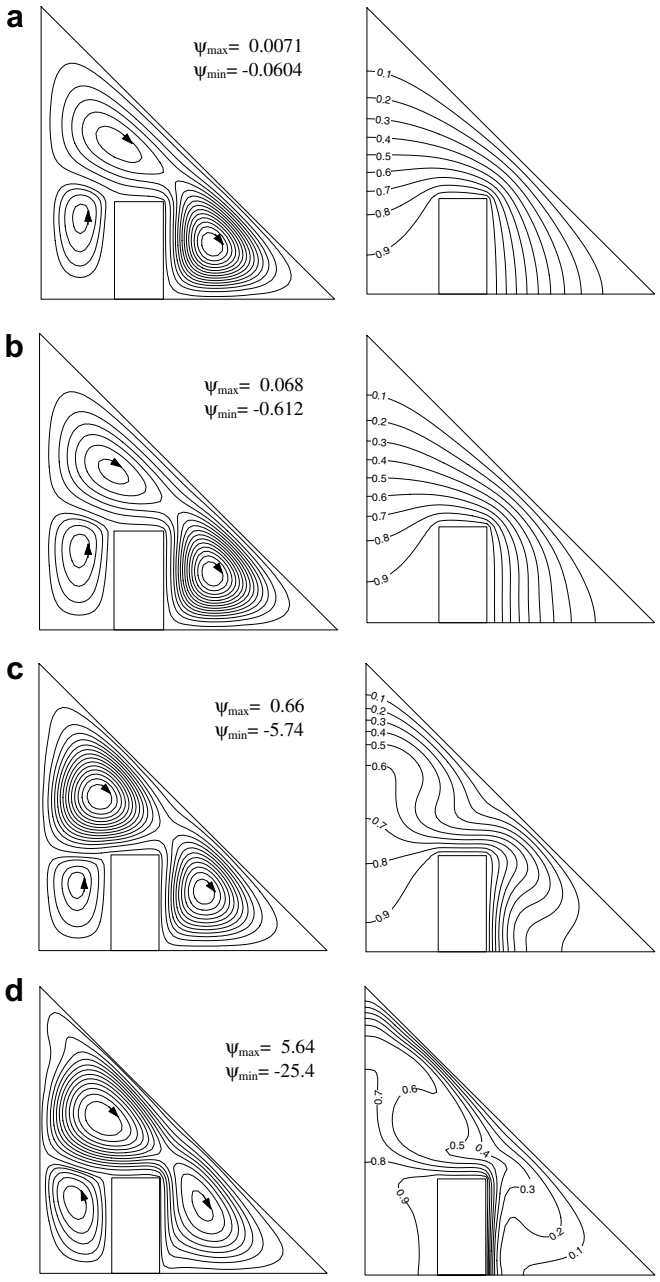

Fig. 4. Streamline (on the left column) and isotherm (on the right column) for different Rayleigh numbers at $c = L/3$, $h = H/3$ and $w = L/6$, $AR = 1.0$. (a) $Ra = 1.0 \times 10^3$, (b) $Ra = 1.0 \times 10^4$, (c) $Ra = 1.0 \times 10^5$, (d) $Ra = 1.0 \times 10^6$.

governing equations in streamline-vorticity form can be obtained via introducing dimensionless variable as follows:

$$X=\frac{x}{L},\quad Y=\frac{y}{L},\quad \Psi=\frac{\psi Pr}{\upsilon},\quad \Omega=\frac{\omega(L)^2 Pr}{\upsilon},\quad \theta=\frac{T-T_c}{T_h-T_c},\quad U,V=\frac{(u,v)L}{\alpha}, \tag{1}$$

$$u=\frac{\partial\psi}{\partial y},\quad v=-\frac{\partial\psi}{\partial x},\quad \omega=\left(\frac{\partial v}{\partial x}-\frac{\partial u}{\partial y}\right),\quad Ra=\frac{\beta g(T_h-T_c)L^3 Pr}{\upsilon^2},\quad Pr=\frac{\upsilon}{\alpha}. \tag{2}$$

Based on the dimensionless variables above governing equations (stream function, vorticity and energy equations) can be written as

$$-\Omega=\frac{\partial^2\Psi}{\partial X^2}+\frac{\partial^2\Psi}{\partial Y^2}, \tag{3}$$

$$\frac{\partial^2\Omega}{\partial X^2}+\frac{\partial^2\Omega}{\partial Y^2}=\frac{1}{Pr}\left(\frac{\partial\Psi}{\partial Y}\frac{\partial\Omega}{\partial X}-\frac{\partial\Psi}{\partial X}\frac{\partial\Omega}{\partial Y}\right)-Ra\left(\frac{\partial\theta}{\partial X}\right), \tag{4}$$

$$\frac{\partial^2\theta}{\partial X^2}+\frac{\partial^2\theta}{\partial Y^2}=\frac{\partial\Psi}{\partial Y}\frac{\partial\theta}{\partial X}-\frac{\partial\Psi}{\partial X}\frac{\partial\theta}{\partial Y}. \tag{5}$$

The physical boundary conditions are illustrated in the physical model (Fig. 1) and they can be defined as follows:

On the inclined wall

$$U=0,\quad V=0,\quad \theta=0. \tag{6}$$

On the bottom and vertical walls

$$U=0,\quad V=0,\quad \frac{\partial\theta}{\partial n}=0. \tag{7}$$

On the heater wall

$$U=0,\quad V=0,\quad \theta=1. \tag{8}$$

3.1. Evaluation of Nusselt number

Heat transfer between isothermal heater (surface-averaged) and inclined wall was computed by local Nusselt number. Integration of local Nusselt number along the heated side of the heater gives mean Nusselt number.

Calculation of local Nusselt number for inclined wall is performed by

$$Nu_n=-\left.\frac{\partial\theta}{\partial n}\right|_{\text{inclined wall}} \tag{9}$$

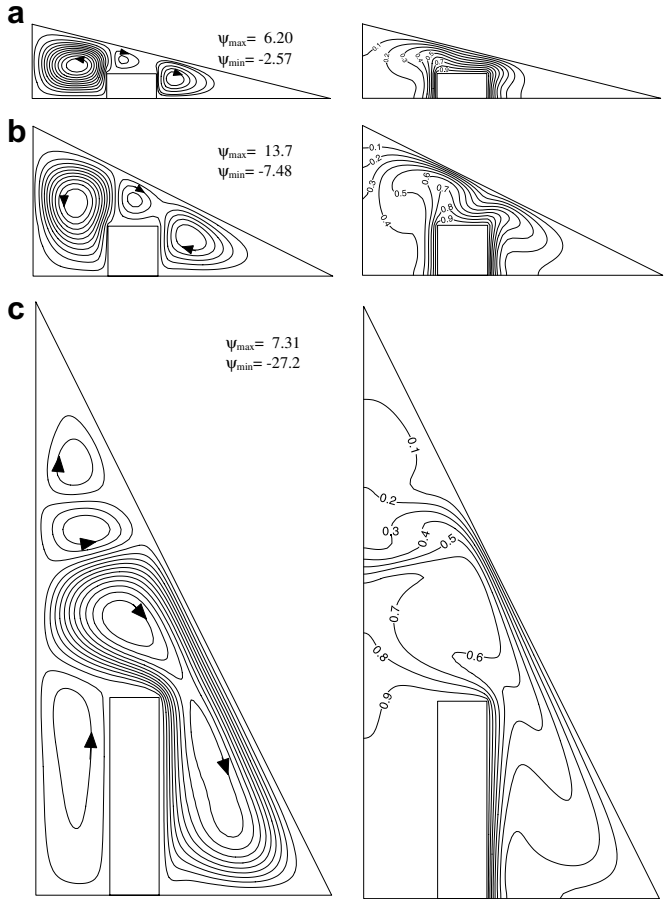

Fig. 5. Streamline (on the left column) and isotherm (on the right column) for different aspect ratios at $Ra=1.0\times10^6$, $c=L/3$, $h=H/3$ and $w=L/6$. (a) AR = 0.25, (b) AR = 0.50, (c) AR = 2.0.

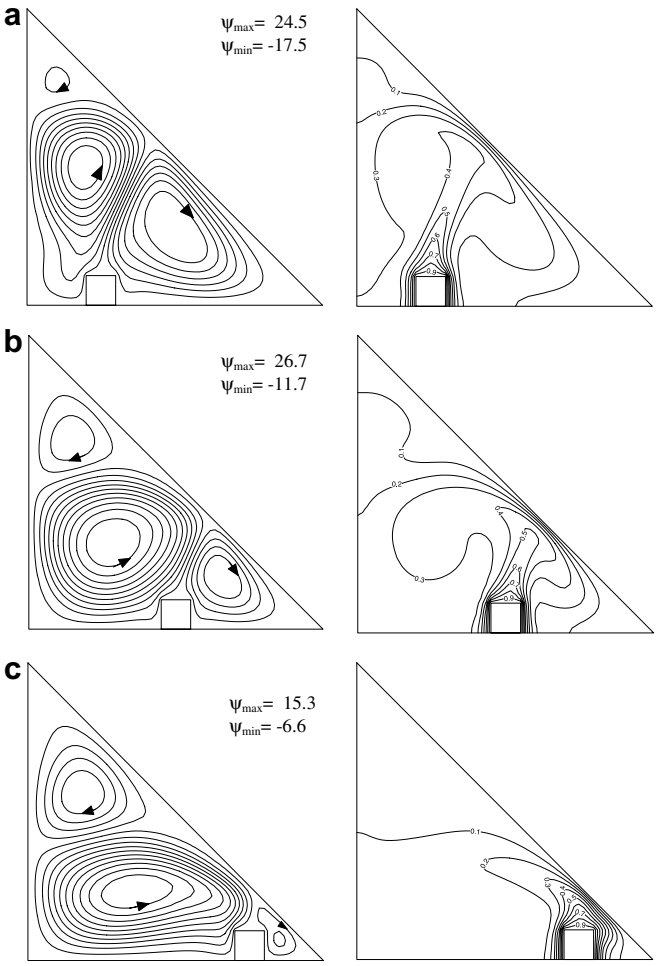

Fig. 6. Streamline (on the left column) and isotherm (on the right column) for different dimensionless location of the heater at $Ra=1.0\times10^6$, AR = 1.0, $h=H/10$, $w=L/10$. (a) $c=1/4L$, (b) $c=1/2L$, (c) $c=3/4L$.

and sides of heater

$$Nu_{n,\text{left side}} = -\left.\frac{\partial\theta}{\partial n}\right|_{\text{left side}}, \quad Nu_{n,\text{right side}} = -\left.\frac{\partial\theta}{\partial n}\right|_{\text{right side}},$$
$$Nu_{n,\text{top side}} = -\left.\frac{\partial\theta}{\partial n}\right|_{\text{top side}}. \tag{10}$$

In these equations "n" shows normal direction on a plane. Average Nusselt numbers for sides of heaters and surface averaged Nusselt numbers are calculated as given by:

$$Nu_{\text{ave left side}} = \int_0^{\text{left top corner}} Nu_{n,\text{left side}}\,\mathrm{d}S,$$
$$Nu_{\text{ave top side}} = \int_{\text{left top corner}}^{\text{right top corner}} Nu_{n,\text{top side}}\,\mathrm{d}S, \tag{11}$$
$$Nu_{\text{ave right side}} = \int_0^{\text{right top corner}} Nu_{n,\text{right side}}\,\mathrm{d}S,$$
$$Nu_{\text{surface averaged}} = Nu_{\text{ave left side}} + Nu_{\text{ave top side}} + Nu_{\text{ave right side}}. \tag{12}$$

3.2. Solution method and numerical tests

Finite difference method is used to solve governing equations (Eqs. (5) and (6)). Central difference method is applied for discretization of equations. The solution of linear algebraic equations was performed using successive under relaxation (SUR) method. As convergence criteria, 10^{-4} is chosen for all depended variables and value of 0.1 is taken for under-relaxation parameter. A regular grid is used in the study and increasing the mesh size from 31×31 to 121×121. Variations of minimum and maximum stream function with grid number are given in Fig. 2. Rectangular mesh of size Δx by Δy is presented in Fig. 1b. The uppermost grid-point on each vertical grid line coincided with the top wall of the triangular enclosure. The inclined wall was approximated with staircase-like zigzag lines. As indicated in the figure, optimum grid dimension is chosen according to variation of $\psi_{\min}$ and $\psi_{\max}$. Thus, it is decided to choose 61×61 grid dimensions. These mesh sizes are sufficient to solve temperature and flow field. For the purpose of the code validation, the natural convection

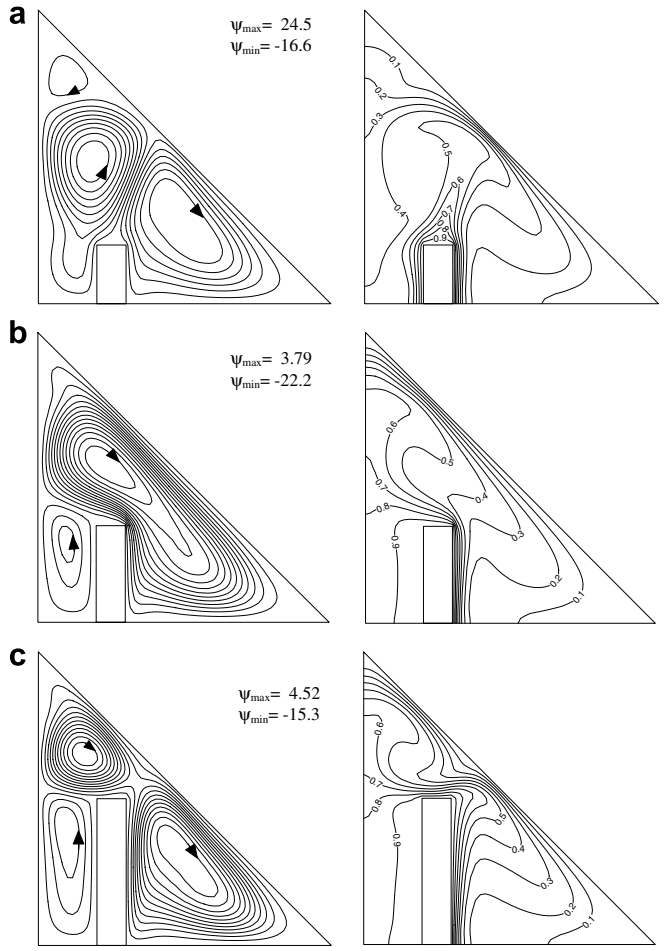

Fig. 7. Streamline (on the left column) and isotherm (on the right column) for dimensionless height of the heater at $Ra = 1.0 \times 10^6$, AR = 1.0, $c = L/4$, $w = L/10$. (a) $h = H/5$, (b) $h = H/3$, (c) $h = H/2$.

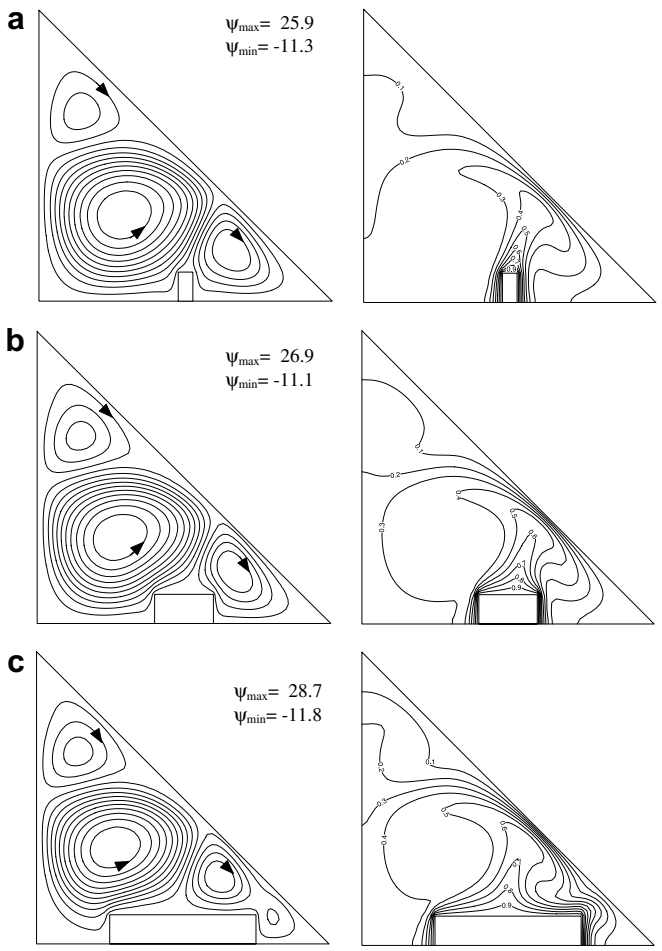

Fig. 8. Streamline (on the left column) and isotherm (on the right column) for dimensionless width of the heater at $Ra = 1.0 \times 10^6$, AR = 1.0, $c = L/2$, $h = H/10$. (a) $w = L/20$, (b) $w = L/5$, (c) $w = L/2$.

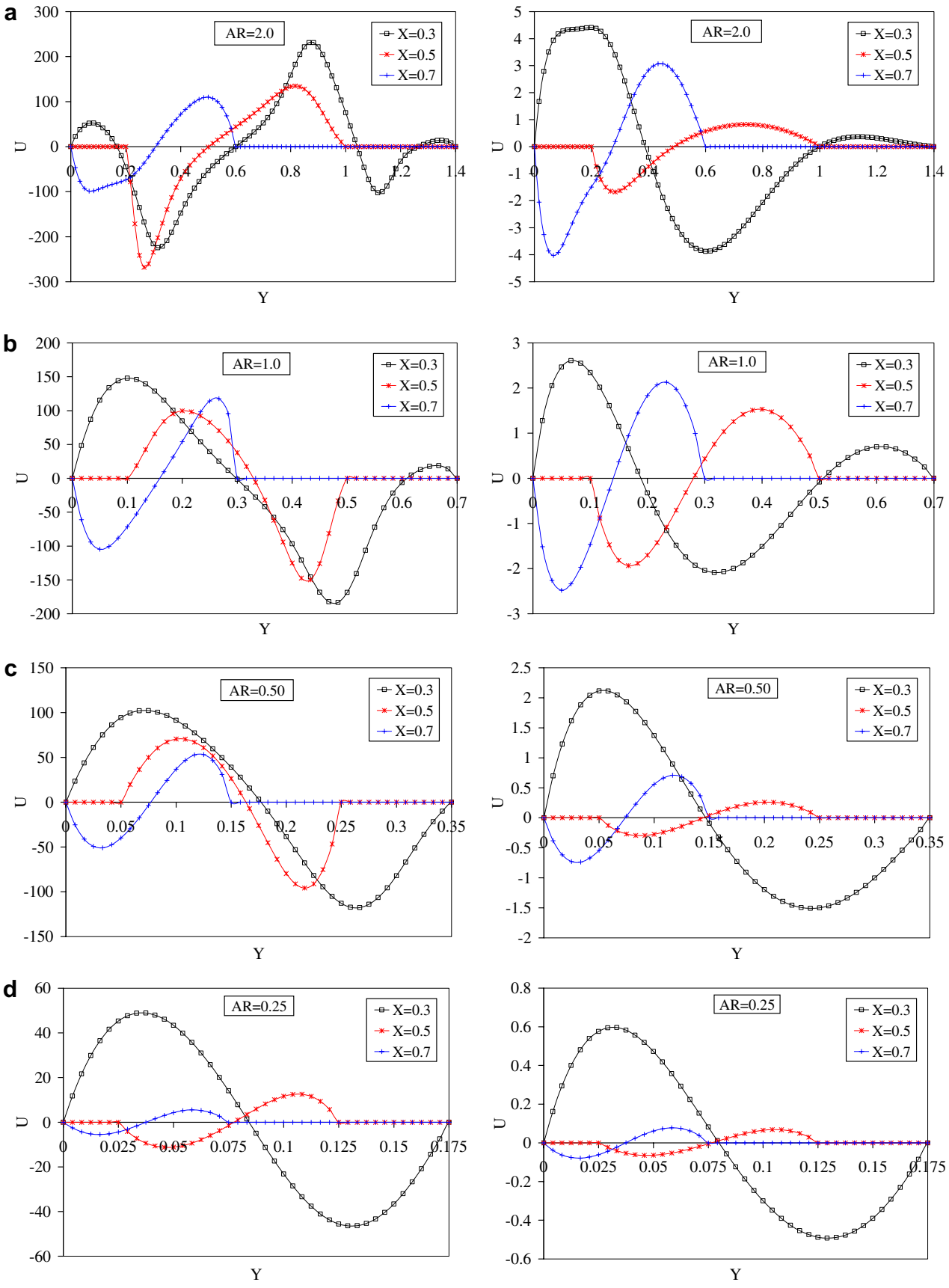

Fig. 9. Velocity profiles at different stations at $Ra = 1.0 \times 10^6$ (on the left column), $Ra = 1.0 \times 10^4$ (on the right column), $c = L/2$, $w = L/6$, $h = H/10$. (a) $A = 2.0$, (b) AR = 1.0, (c) AR = 0.50, (d) AR = 0.25.

problem in a triangle enclosure without a heater was tested at $Ra = 2772$ with the results of literature [4,6,7]. In these studies, the bottom and inclined walls are heated and cooled, respectively. The calculated mean Nu numbers for the test case are compared and plotted in Fig. 3. The values are in good agreement with previously calculated values. Contours of streamline and isotherms are almost the same as those given in the literature for a rectangular enclosure but they are not presented here to save space.

4. Results and discussion

A numerical study has been performed through finite difference method to analyze the laminar natural convection heat transfer and fluid flow in triangular enclosure due to heater insertion. The temperature of the inclined wall of enclosure is lower than the temperature of the heater. Effective parameters such as Rayleigh number, heater height, heater width, heater location center and aspect ratio of triangular enclosure on heat transfer and fluid flow were analyzed. We presented the results in two sections. The first

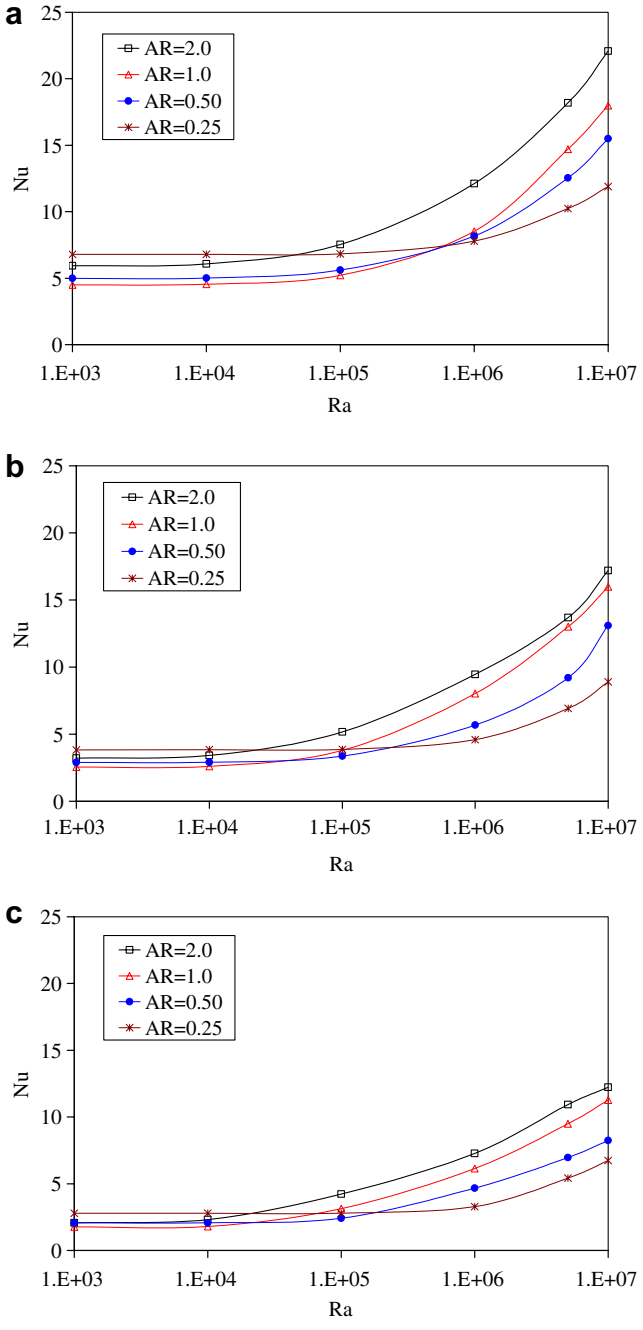

Fig. 10. Surface-averaged Nusselt number at the heater as a function of Ra number for different AR for $c = L/2$, $w = L/6$. (a) $h = H/3$, (b) $h = H/5$, (c) $h = H/10$.

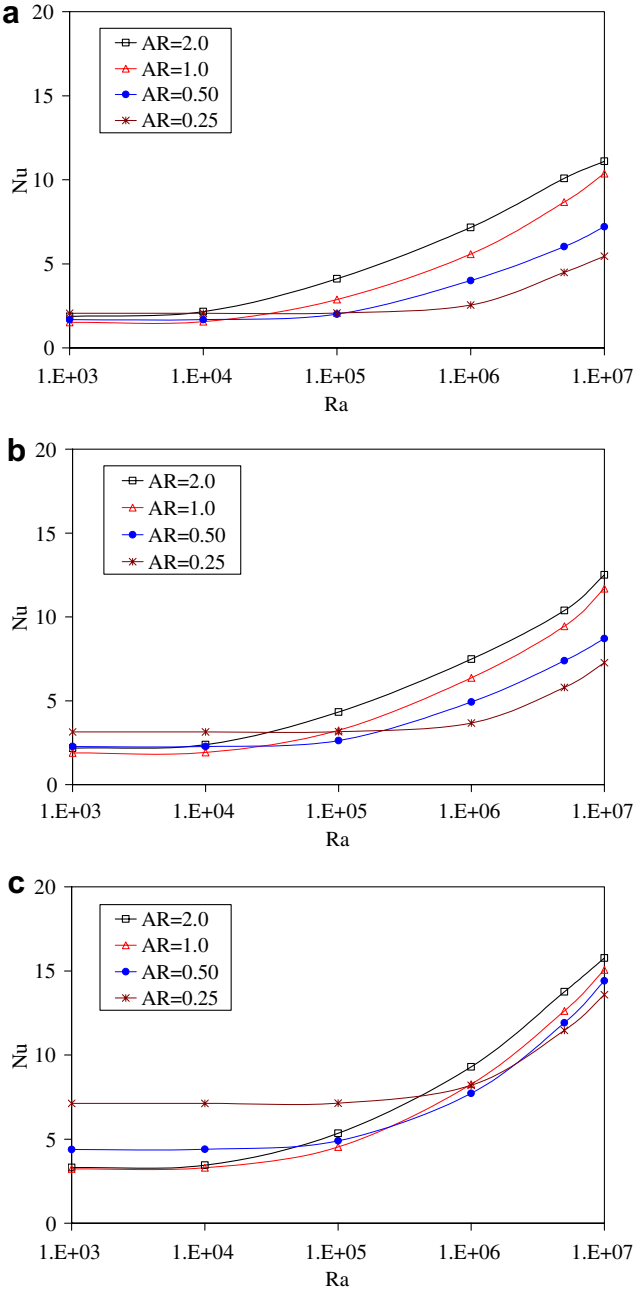

Fig. 11. Surface-averaged Nusselt number at the heater as a function of Ra number for different AR for $c = L/2$, $h = H/10$. (a) $w = L/10$, (b) $w = L/5$, (c) $w = L/2$.

section will focus on flow and temperature fields, which contents streamlines, isotherms and velocity profiles for mentioned cases. The following section will discuss heat transfer including variation of local and mean Nusselt numbers.

4.1. Flow and temperature fields

Flow and temperature fields are simulated using streamlines and temperature contours for selected parameters of flow, heater and geometry. Effects of Rayleigh number on streamlines (on the left) and isotherms (on the right) are presented in Fig. 4 for $c = L/3$, $h = H/3$, $w = L/6$ and AR = 1. Visualizations are given from $Ra = 10^3$ to $Ra = 10^6$. It can be seen from the figure that three vortices are formed for all values of Rayleigh number because heated air moves up from the heater and impinges to the cold inclined wall. In Fig. 4a, a vortex is formed between left side of the heater and insulated vertical wall of triangular enclosure which rotates in counterclockwise (CCW) direction. Its shape and length are almost same for all Rayleigh number. Other two cells are obtained on the top of heater and right corner of the triangle enclosure. These are very similar for $Ra = 10^3$ (Fig. 4a) and $Ra = 10^4$ (Fig. 4b) due to quasi-conductive regime. As indicated by De Vahl Davis and Jones [2] heat transfer is largely by conduction for $Gr < 10^4$. Both top and right vortices rotate in clockwise (CW) direction due to rising fluid from heater to inclined wall. It rises and replaces with cooled fluid. The eye of vortices becomes almost in the same place with the increasing of Rayleigh number. Maximum and minimum stream function values are shown on the corner of the streamline figure. They indicated that the strength of the flow increases with increasing Rayleigh number. Streamlines are more packed at the right side of the heater. It means that the flow moves faster as natural convection is intensified. As Rayleigh number increases, velocity of fluid at the top of heater also increases due to increasing of effects of convection heat transfer regime in Fig. 4c and d. Increasing of Rayleigh number causes a denser clustering of isotherms. This will lead to lower heat transfer levels. Similar results can be seen in the studies of Acharya and Moukalled [23,24].

Aspect ratio (AR) of the triangular enclosure is important parameter for flow and temperature fields. We defined the aspect ratio as the ratio of the height of the vertical wall to the length of the bottom wall of the enclosure ($AR = H/L$) which changes from 0.25 to 2 along the present paper. Thus, Fig. 5a–c presents the effect of AR on streamlines (on the left) and isotherms (on the right) with the same dimensionless height ($h = H/3$) and width ($w = L/6$) of the heater at $c = L/3$ and $Ra = 10^6$ for the value of AR = 0.25, 0.5 and 2. Three vortices are observed for AR = 0.25 and AR = 0.5 (Fig. 5a and b). The top and right one rotate in CW while left one in CCW. On the other hand, five vortices are formed for the highest AR due to small angled corner and the flow squeezes in that part. Values of stream functions show that the strength of flow becomes stronger with increasing AR. The flow separates as a jet stream from the right side toward the top of the heater. Isotherms (on the right) show that increasing of AR causes heat transfer to decrease because of the distance between heater and the inclined cold wall. Plume-like flow temperature distribution is observed for AR = 0.5 (Fig. 5b).

Fig. 6a–c is presented to see the effect of heater location on flow and temperature distribution with the parameters of $Ra = 10^6$, AR = 1, $w = L/10$, $h = H/10$. As can be seen from the figure that two big and one small cell are obtained for all cases. When c is equal to $L/4$ (Fig. 6a), which is close to

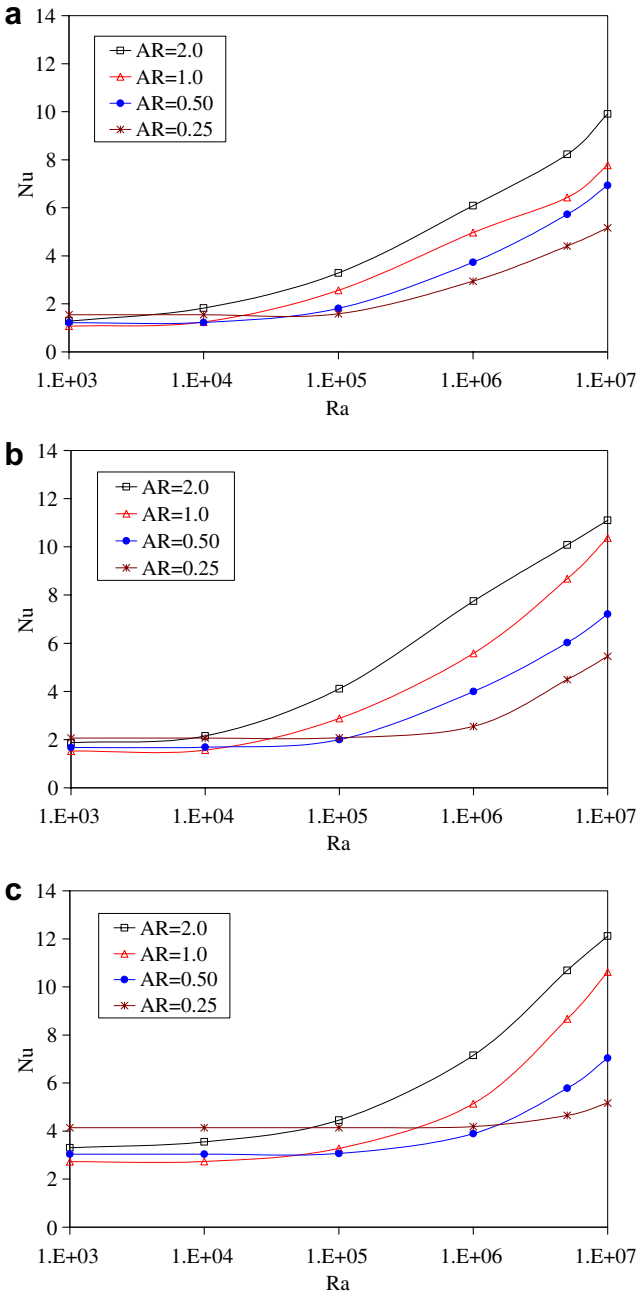

Fig. 12. Surface-averaged Nusselt number at the heater as a function of Ra number for different AR for $h = H/10$, $w = L/10$. (a) $c = 1/4L$, (b) $c = 1/2L$, (c) $c = 3/4L$.

vertical adiabatic wall, left cell rotates in CCW and the other one in clockwise. Other very small cell placed on the top of enclosure and rotates in CW. Their intersections locate on the top of heater. In this case, the problem represents natural convection in enclosures heated from below which is studied earlier by Aydin and Yang [11]. When heater locates on the middle of the bottom wall (Fig. 6b), the cell on the top becomes bigger when it is compared with the one given in Fig. 6a. For $c = 3/4L$ (Fig. 6c), the configuration of flow completely change because heater and inclined cold walls are very close to each other. Thus, the eye of the main vortex is formed almost on the middle of the enclosure and it rotates in CCW (Fig. 6c). The CCW rotation of flow indicates that it moves up along the left side of the heater and impinges to the inclined walls and separates. Another big cell forms on the top corner in CW direction. Minimum values of stream function are increased with the increasing of c. However, when heater locates near the right corner, the smallest value of maximum stream function is obtained. Plumelike temperature distribution is formed from the heated block to the inclined wall due to convection regime of heat transfer. Changing of the location of the heater affects the direction of plumelike distribution. When heater locates near the right corner of the enclosure, almost the temperature of half of the enclosure equals to inclined wall temperature. Effects of the height of the heater in enclosures are given in Fig. 7a–c for AR = 1, $Ra = 10^6$, $c = L/4$ and $w = L/10$. It is observed that the height of heater directly affects the temperature and flow field. For $h = H/5$ (Fig. 7a), flow and temperature fields are very similar to Fig. 6. However, when h is equal to $H/3$ (Fig. 7b), the result resembles to the Fig. 4; however two vortices are formed due to thinner heater in this case. The stronger vortex is located close to the top wall of heater and a jetlike flow forms at the right corner of the heater. When $h = H/2$ (Fig. 7c), the flow separates between right and top of the heater. Thus, three vortices are formed. In the case of higher heater length, the flow and temperature distribution behave as differentially heated enclosure. (Fig. 7b and c). However, for $h = H/5$, mushroom shaped isotherms are formed. It means that, heat transfer at the top of the heater is very effective.

Another important parameter is the width of the heater. Obtained results for this parameter are presented in Fig. 8a–c for the fixed parameters as $Ra = 10^6$, $h = H/10$, $c = L/2$ and AR = 1. As can be seen from the figure, the dimensionless width of the heater is not an effective parameter on flow strength. However, strong plumelike flow is observed with the increasing of the heater width.

Horizontal velocity profiles are presented in Fig. 9a–c for $Ra = 10^4$ (on the right) and $Ra = 10^6$ (on the left) at

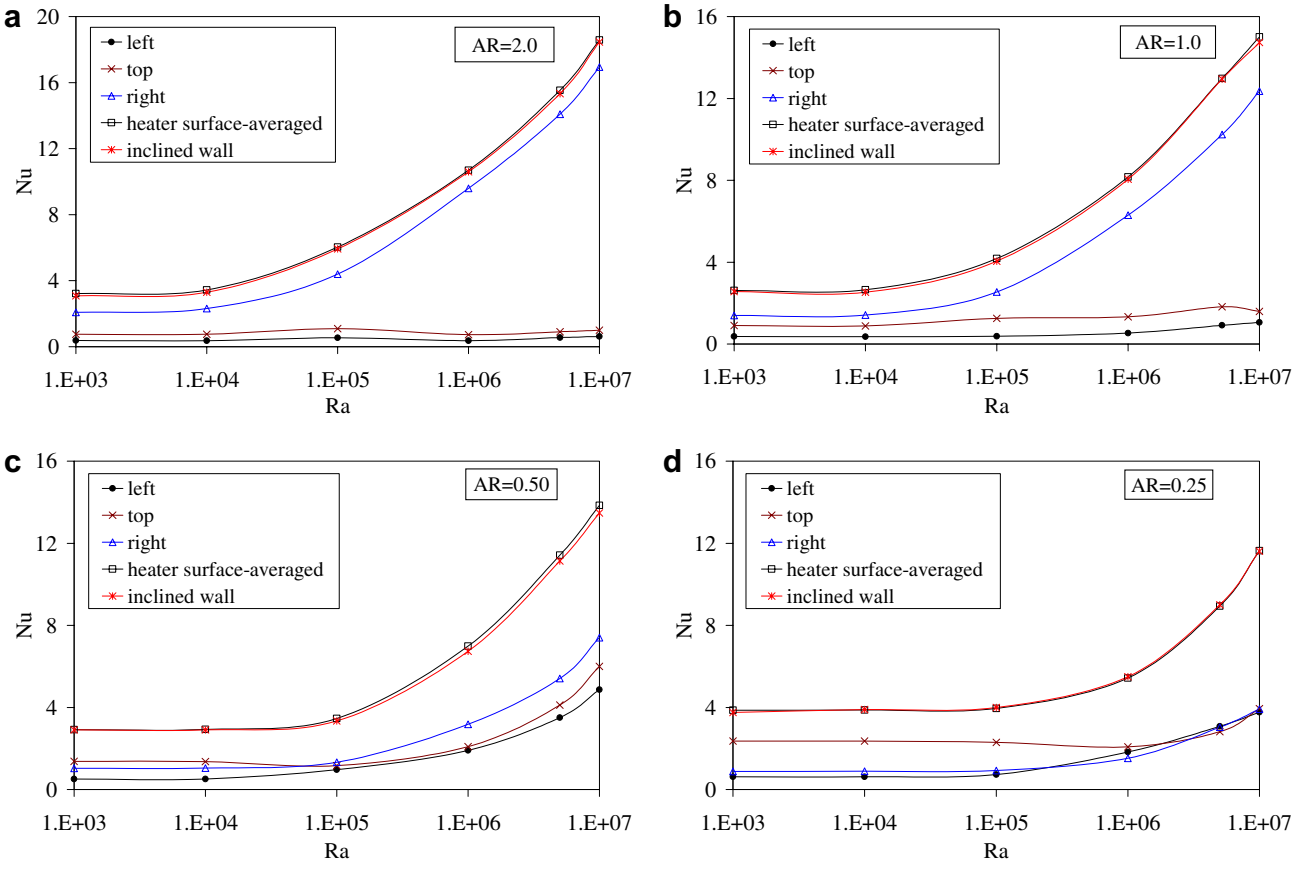

Fig. 13. Surface-averaged Nusselt number as a function of Ra number at $c = L/3$, $h = H/3$, $w = L/6$. (a) AR = 2.0, (b) AR = 1.0, (c) AR = 0.50, (d) AR = 0.25.

different ARs. Profiles are plotted along the vertical direction at three different location in x-direction as $x = 0.3$, 0.5 and 0.7. Other governing parameters chosen as $c = L/2$, $w = L/6$ and $h = H/10$. As expected, the values of velocities are increased with increasing of Rayleigh number. At $Ra = 10^4$, the flow is weak due to quasi-conduction dominant heat transfer regime. Meanwhile, values of velocities decrease with decreasing of AR. For $Ra = 10^6$ and AR = 2, maximum positive and negative values are almost equal to each other for $0.2 < Y < 1$. Sinusoidal velocity profiles are obtained on the heater for all parameters. Again, for $Ra = 10^6$, sinusoidal variation is obtained at all stations in x-direction for AR = 0.25 and 0.5.

4.2. Heat transfer

Variation of surface-averaged Nusselt number with Rayleigh number for different ARs and heater height are presented in Fig. 10a–c at $w = L/6$ and $c = L/2$. Surface-averaged Nusselt number is calculated by integration of local Nusselt number over heater surface as given in Eq. (10). Fig. 10 is given for different dimensionless height ratio of the heater. As given in the figure, Nusselt numbers are almost constant up to $Ra = 10^4$ due to quasi-conductive regime. After that they increase with the increasing of Rayleigh number as expected. When Figs. 10a–c are compared with each other, it is seen that, Nusselt number is decreased with decreasing of heater height due to decreasing of heater surface, which is also supported for isothermal heaters by Dagtekin and Oztop [14]. For the fixed parameters, higher heat transfer is formed for higher values of AR. The best heat transfer is observed for the case of $c = L/2$, $w = L/6$, $h = H/3$ and the highest Rayleigh number. Effects of the width of the heater on heat transfer as a function of Rayleigh number and AR for $c = L/2$ and $h = H/10$ are presented in Fig. 11. As expected, increasing width length of the heater enhances the heat transfer. When conduction heat transfer is dominant (at small Ra number), higher heat transfer is obtained for the lower AR. On the contrary, heat transfer increases with increasing of AR for the highest Rayleigh number. Quasi-conductive regime is validated up to $Ra < 10^5$ for the smallest AR and the highest heater width due to increasing heated surface area between hot and cold walls.

Fig. 12a–c show surface averaged-Nusselt number for $c = L/4$, $c = L/2$ and $c = 3/4L$, respectively. Results are presented for different Rayleigh numbers and ARs. Nusselt numbers reflect the temperature distribution presented in Fig. 6a–c (on the right column). At $c = L/4$, Nusselt numbers decrease with decreasing AR and also same trend is shown in Fig. 12b. On the contrary, when $c = 3/4L$ (Fig. 12c), Nusselt number is higher for AR = 0.25 than other AR values of local Nusselt numbers at low Rayleigh numbers due to very small inner volume of the triangular enclosure. Thus, conduction heat transfer becomes stronger than convection heat transfer. At the highest Rayleigh numbers again same trend is obtained as given in Fig. 12a and b. When figures are compared, it can be seen that if heater locates near the right corner, heat transfer enhances, except AR = 1, due to short distance between hot and cold walls for all Rayleigh numbers.

Fig. 13a–d illustrates the variations of the mean Nusselt number with Rayleigh number for left, right and top side of the heater at different ARs. Also, it shows a comparison between surface-averaged and inclined wall Nusselt numbers. In this case, the parameters are: $c = L/3$, $h = H/3$

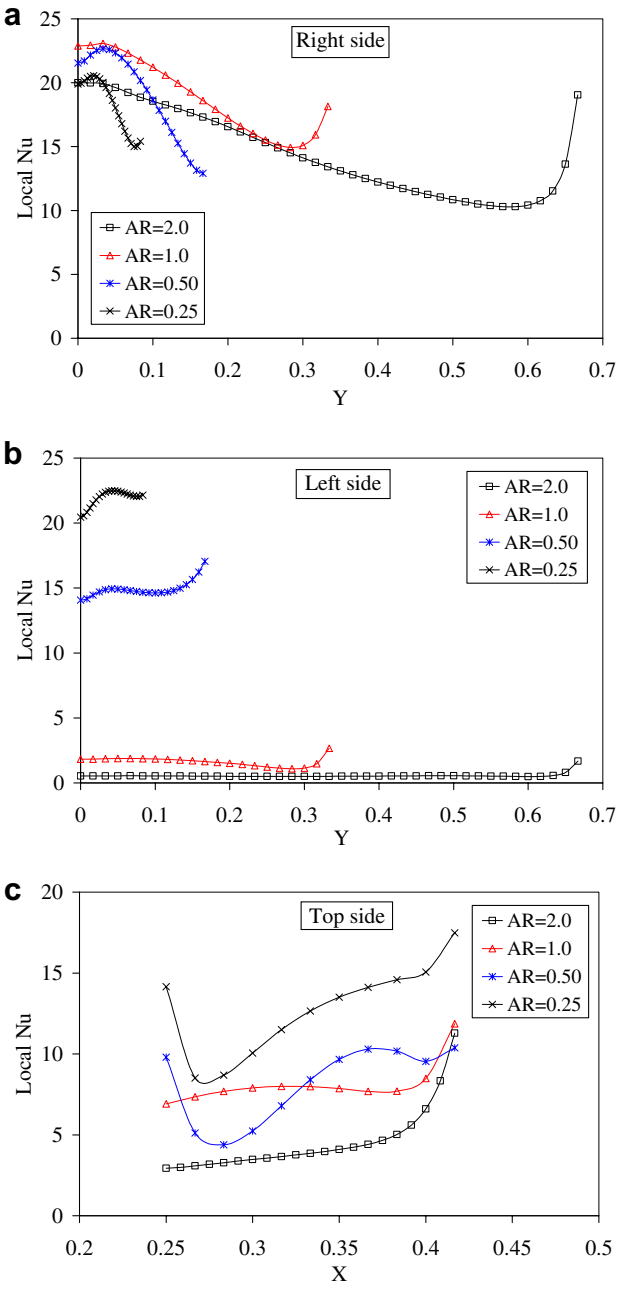

Fig. 14. Variation of local Nusselt number along the heater wall for different aspect ratios at $Ra = 1.0 \times 10^6$, $c = L/3$, $h = H/3$, $w = L/6$. (a) Right side, (b) left side, (c) top side.

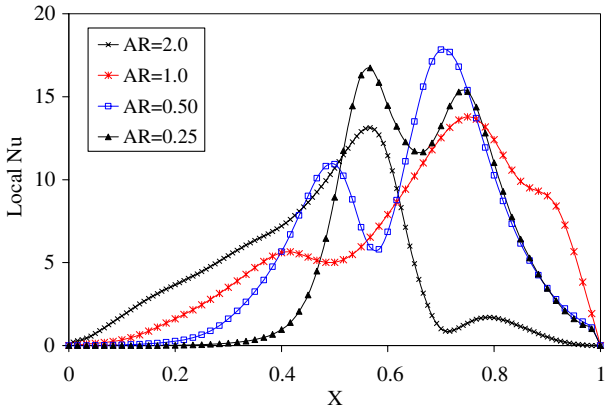

Fig. 15. Variation of local Nusselt number along the inclined wall for different aspect ratios at $Ra = 1.0 \times 10^6$, $c = L/3$, $h = H/3$, $w = L/6$.

and $w = L/6$. It is observed that values of Nusselt numbers become constant up to $Ra = 10^4$ due to quasi-conductive regime. For higher ARs including AR = 2.0 and AR = 1.0 (Fig. 13c and d), mean Nusselt number becomes constant for all Rayleigh number on the top and left side of the heater due to long distance between hot and cold walls. Most of the heat transfer takes place through the right wall for AR = 1.0 and AR = 2.0. Also small contribution of the left wall to overall heat transfer in all cases is due to the fact that this lies adjacent to a corner where two adiabatic walls intersect. However, Nusselt number increases with increasing of Rayleigh numbers, which is expected. When AR = 0.5 and 0.25 (Fig. 13a and b), an increase is observed in Nusselt number for all sides of the heater due to decreasing volume. All figures show that surface-averaged Nusselt number and inclined wall Nusselt number equals to each other. It means that energy input and output is equal in the present system.

Local Nusselt number (LNN) distributions along the sides of the heater are shown in Fig. 14 for different ARs. Variations of LNN on the right side of the heater are given in Fig. 14a. It has the same trend and a minimum value around the top of the heater for all ARs. However, a maximum value is obtained near the bottom wall of the heater. Left side of the heater is strongly affected by the variation of the ARs (Fig. 14b). The LNN values become almost constant and very small for AR = 2.0 and AR = 1.0. Their values increase with the decrease of AR due to lower fluid velocity and long distance between hot and cold walls. On the top of heater, the trends of LNN values are very similar for AR < 1. They increase almost linearly and become maximum at the right edge of the heater. However, when $AR \geqslant 1$ again curves show similar trend. They have minimum value near the left edge. Variations of LNN along the inclined cold wall for different AR and $h = H/3$, $c = L/3$, $w = L/6$ and $Ra = 10^6$ are shown in Fig. 15. LNN distribution show wavy trend along the wall. Peak values are observed due to impingement of the flow negotiating around the heater. Figs. 14 and 15 refer to the counter plot of Figs. 4–8. Higher heat transfer occurred at the locations of flow-separation points. The highest and lowest peak values are observed for AR = 0.5.

5. Conclusions

In these analyses, the results of the study of natural convection in two-dimensional triangular enclosure for steady-state regime with protruding heater and cooling from inclined wall are presented using main parameters of interest as Rayleigh number, heater height, heater width, heater location and aspect ratio.

In view of the obtained results, following findings may be summarized:

(1) Nusselt number becomes constant for the smaller values of Rayleigh numbers and aspect ratio of the triangular enclosure due to domination of quasi-conductive regime, Nusselt number increases with the increasing of Rayleigh number.
(2) It is observed that the location and height of the heater are one of the most important parameters on flow and temperature fields and heat transfer. Increased heater height, as expected, enhances the heat transfer due to increasing heated surfaces.
(3) Although the width of the heater is not an effective parameter on flow field, it has an important effect on heat transfer due to increasing of heater surface.
(4) Peak values on local Nusselt number distributions are observed on the top of the heater and they show wavy variation.
(5) Flow strength is decreased for AR > 1 due to increasing distance between hot and cold walls depending on the geometrical parameters of the heater. Further, an optimization study may be useful but it is out of the scope in the present study.
(6) Heat transfer is very weak at the left and top side of the heater when it is compared with the right side of the heater.
(7) To obtain better heat removal from the heater, higher aspect ratio must be chosen and the heater must be located to the center of the bottom wall.

In the future, the study can be extended for turbulent flow using different fluids, different thermal boundary conditions such as constant heat flux or radiation and unsteady flow. An optimization study can be performed; however, it is out of the scope of this paper.

References

[1] B. Gebhart, Y. Jaluria, R.L. Mahajan, B. Sammakia, Buoyancy-induced Flows and Transport, Hemisphere, Washington, DC, 1988.
[2] G. De Vahl Davis, I.P. Jones, Natural convection of air in a square cavity: a comparison exercise, Int. J. Numer. Methods Fluids 3 (1983) 227–248.
[3] S. Ostrach, Natural convection in enclosures, J. Heat Transfer 110 (1988) 1175–1190.

[4] S.C. Tzeng, J.H. Liou, R.Y. Jou, Numerical simulation-aided parametric analysis of natural convection in a roof of triangular enclosures, Heat Transfer Eng. 26 (2005) 69–79.
[5] H. Asan, L. Namli, Laminar natural convection in a pitched roof of triangular cross-section: summer day boundary conditions, Energy Build. 33 (2000) 69–73.
[6] H. Asan, L. Namli, Numerical simulation of buoyant flow in a roof of triangular cross section under winter day boundary conditions, Energy Build. 33 (2001) 753–757.
[7] V.A. Akinsete, T.A. Coleman, Heat transfer by steady laminar free convection in triangular enclosures, Int. J. Heat Mass Transfer 25 (1982) 991–998.
[8] E.H. Ridouane, A. Campo, M. Hasnaoui, Benefits derivable from connecting the bottom and top walls of attic enclosures with insulated vertical side walls, Numer. Heat Transfer Part A 49 (2006) 175–193.
[9] Y. Varol, A. Koca, H.F. Oztop, Natural convection in a triangle enclosure with flush mounted heater on the wall, Int. Comm. Heat Mass Transfer 33 (2006) 951–958.
[10] Y. Varol, A. Koca, H.F. Oztop, Natural convection in a Gambrel Roofs, Build. Environ. 42 (2007) 1291–1297.
[11] O. Aydin, W.J. Yang, Natural convection in enclosures with localized heating from below and symmetrical cooling from sides, Int. J. Numer. Meth. Heat Fluid Flow 10 (2000) 518–529.
[12] H. Turkoglu, N. Yucel, Effect of heater and cooler locations on natural convection in square cavities, Numer. Heat Transfer Part A 27 (1995) 351–358.
[13] Y. Varol, A. Koca, H.F. Oztop, Natural convection in a shed roof with eave: Comparison of summer and winter days boundary conditions, in: Proceedings of the 2nd International Green Energy Conference, Canada, 2006, pp. 1440–1450.
[14] I. Dagtekin, H.F. Oztop, Natural convection heat transfer by heated partitions within enclosure, Int. Comm. Heat Mass Transfer 40 (2001) 823–834.
[15] S.H. Chuang, J.S. Chiang, Y.M. Kuo, Numerical simulation of heat transfer in a three-dimensional enclosure with three chips in various position arrangements, Heat Transfer Eng. 24 (2003) 42–59.
[16] M.T. Bhoite, G.S.V.L. Narasimham, M.V.K. Murthy, Mixed convection in a shallow enclosure with a series of heat generating components, Int. J. Thermal Sci. 44 (2005) 121–135.
[17] A. Ben-Nakhi, A.J. Chamkha, Natural convection in inclined partitioned enclosures, Heat Mass Transfer 42 (2006) 311–321.
[18] N. Yucel, A.H. Ozdem, Natural convection in partially divided square enclosure, Heat Mass Transfer 40 (2003) 167–175.
[19] X. Shi, J.M. Khodadadi, Laminar natural convection heat transfer in a differentially heated square cavity due to a thin fin on the hot wall, J. Heat Transfer 125 (2003) 624–634.
[20] S.H. Tasnim, M.R. Collins, Numerical analysis of heat transfer in a square cavity with a baffle on the hot wall, Int. Comm. Heat Mass Transfer 31 (2004) 639–650.
[21] E. Bilgen, Natural convection in enclosures with partial partitions, Renew. Energy 26 (2002) 257–270.
[22] E. Bilgen, Natural convection in cavities with a thin fin on the hot wall, Int. J. Heat Mass Transfer 48 (2005) 3493–3505.
[23] F. Moukalled, S. Acharya, Natural convection in a trapezoidal enclosure with offset baffles, J. Thermophys. Heat Transfer 15 (2001) 212–218.
[24] F. Moukalled, S. Acharya, Natural convection in trapezoidal cavities with baffles mounted on the upper inclined surfaces, Numer. Heat Transfer Part A 37 (2000) 545–565.
[25] Y. Liu, N.P. Thien, An optimum spacing problem for three chips mounted on a vertical substrate in an enclosure, Numer. Heat Transfer Part A 37 (2000) 613–630.
[26] A. Ben-Nakhi, A.J. Chamkha, Effect of length and inclination of a thin fin on natural convection in a square enclosure, Numer. Heat Transfer Part A 50 (2006) 389–407.
[27] T. Icoz, Y. Jaluria, Numerical simulation of boundary conditions and the onset of instability in natural convection due to protruding thermal sources in an open rectangular channel, Numer. Heat Transfer Part A 48 (2005) 831–847.
[28] C.G. Rao, A.V. Krishna, P.N. Srinivas, Simulation studies on multimode heat transfer from a square-shaped electronic device with multiple discrete heat sources, Numer. Heat Transfer Part A 48 (2005) 427–446.
[29] H.F. Oztop, E. Bilgen, Natural convection in differentially heated and partially divided square cavities with internal heat generation, Int. J. Heat Fluid Flow 27 (2006) 466–475.